Met. Mater. Int., Vol. 20, No. 4 (2014), pp. 765~773
doi: 10.1007/s12540-014-4022-1

Ab-initio Study of the Structural, Electronic, Elastic and Vibrational Properties of the Intermetallic Pd_3V and Pt_3V Alloys in the $L1_2$ Phase

N. Arıkan[1,*], A. İyigör[2], A. Candan[2], M. Özduran[3], A. Karakoç[3], Ş. Uğur[4], G. Uğur[4], A. Bouhemadou[5], S. Bin-Omran[6], and N. Guechi[5]

[1]Ahi Evran University, Education Faculty, Science Education Department 40100 Kırşehir, Turkey
[2]Ahi Evran University, Central Research and Practice Laboratory (AHÝLAB.), 40100 Bağbaşı-Kırşehir, Turkey
[3]Ahi Evran University, Department of Physics, Faculty of Arts and Sciences, 40100Bağbaşı-Kırşehir, Turkey
[4]Gazi University, Department of Physics, Faculty of Science, 06500 Ankara-Turkey
[5]University Setif 1Laboratory for Developing New Materials and their Characterization, Department of Physics, Faculty of Science, Setif 19000, Algeria
[6]King Saud University, Department of Physics and Astronomy, College of Science, P.O. Box 2455, Riyadh 11451, Saudi Arabia

(received date: 24 July 2013 / accepted date: 8 November 2013)

Pseudopotential plane-wave method based on density functional theory within the generalized gradient approximation for the exchange-correlation potential has been applied to study the structural, electronic, elastic and vibrational properties of the binary intermetallic Pd_3V and Pt_3V in the $L1_2$ phase. The optimized lattice constant, bulk modulus and its pressure derivative, independent single-crystal elastic constants and elastic wave velocities in three different directions are evaluated and compared with the available experimental and theoretical data. The polycrystalline elastic parameters, hardness coefficient, elastic anisotropy, Debye temperature are estimated. The electronic band structure, electronic total and partial densities of states, and total magnetic moment of the Pd_3V and Pt_3V alloys are computed and analyzed in comparison with the existing theoretical and experimental findings. Phonon-dispersion curves and their corresponding total and projected densities of states were obtained for the first time using a linear-response in the framework of the density functional perturbation theory.

Keywords: intermetallics, crystal structures, mechanical properties, thermodynamic properties

1. INTRODUCTION

With the increasing demand for structural materials that can withstand severe oxiding environments and high operating temperatures, many intermetallic compounds have been investigated to test their feasibility in the last two decades [1]. Pd and Pt based alloys are important intermetallic materials with application as stable, medical, thermoelectric and electrode devices. Pd_3V and Pt_3V alloys belong to the binary intermetallic family. These two compounds can crystallize in two different crystalline structures: $L1_2$ and $D0_{22}$ phases. The $D0_{22}$ phase is more stable than the $L1_2$ one [2,3]. However, the $L1_2$ structure is significantly more ductile than the $D0_{22}$ structure [2]. Structural, electronic, thermodynamic, elastic, magnetic, structural stability, cohesive properties and phase diagrams of the Pd_3V and Pt_3V alloys have been the subject of various experimental and theoretical investigations [2-19]. Theoretically, using the linear muffin-tin orbitals (LMTO) method based on the density functional theory (DFT), Lebacq *et al*. [3] studied the electronic structure, cohesive properties and phase stability of the Pd_3V and Pt_3V alloys. The structural stability, electronic and elastic properties of the $L1_2$-ordered intermetallic phase Pd_3V was studied in the framework of the DFT within the GGA by Wang *et al*. [4]. Hirschl *et al*. [5] calculated the electronic structure of Pd_3V in the $L1_2$ phase via DFT. Lu *et al*. [6] showed that spin-polarized electronic structure calculations are crucial for predicting the correct T=0 crystal structures for the Pd_3V and Pt_3V alloys. Wolverton and Zunger [7], using first-principles calculations, reported that the density of states at the Fermi level ($N(E_F)$) for the Ni_3V and Pd_3V in $L1_2$ phase is significantly higher than their $N(E_F)$ in the $D0_{22}$ phase. Tobola and Pécheur [8], using the KKR method, showed that the ground state proper-

*Corresponding author: nihat.arikan@hotmail.com

ties of the Pd_3V alloy in the $L1_2$ phase is magnetic. On the experimental side, Brown *et al*. [9] measured the valance electronic band structure of the Pt_3V compound in its $L1_2$ phase by means of the synchrotron radiation ultraviolet photoemission. The electronic structure of Pt_3V surface was measured using the valance-band photoelectron spectroscopy by Mun *et al*. [10]. The resistivity, low temperature magnetization and susceptibility of Pd_3V were measured by Sheikh and Williams [11]. Cabet *et al*. [12] studied the phase stability and electronic structure of the Pd_3V and Pt_3V alloys by means of the transmission electronic microscopy.

Despite the numerous interesting experimental and theoretical studies on physical properties of the Pd_3V and Pt_3V alloys, which were reported in past years [2-19], some of their physical properties are still not yet investigated or not well-established such as their mechanical behavior, which has been investigate only for Pd_3V, and vibrational properties. It is well known that knowledge of the elastic properties of a material is important due to their closely relations with various physical fundamental properties. In particular, they provide information on the stability and stiffness of the material against externally applied strains. Measurements of elastic parameters are generally difficult, so the lack of experimental data can be compensated by theoretical simulation based on accurate *ab-initio* theories. So, the first main objective of the present work is to determine the elastic constants and their related properties for these two materials under consideration. The full phonon-dispersion curves are necessary for a microscopic understanding of the lattice dynamics. The knowledge of the phonon spectra plays a significant role in the determination of various material properties such as phase transition, thermodynamic stability, transport and thermal properties. So, the study of the vibrational properties of the Pd_3V and Pt_3V alloys in the $L1_2$ phase constitutes the second main objective of the present work.

Computer modeling of materials based on accurate *ab-intio* methods has been a driving issue in the prediction of materials' properties and provides an important tool to explore some properties which are not yet experimentally investigated or are difficult to be explored experimentally. Thus, we have performed pseudopotential plane-wave *ab-initio* calculations of a wide range of physical properties of Pd_3V and Pt_3V. The herein reported results include the optimized crystalline parameters, monocrystalline and polycrystalline elastic moduli, and their related properties, electronic band structure and their corresponding densities of states, phonon dispersions and their corresponding densities of states, and temperature dependence of the specific heat at constant volume.

The rest of this paper is organized as follows. After this introduction, a brief description of the computational methods and details are given in section 2. The results of our total energy *ab-initio* calculations are presented and discussed in section 3. We then summarize and conclude in section 4.

2. COMPUTATIONAL DETAILS

All herein done total energy calculations were carried out using a pseudopotential plane-wave (PP-PW) scheme within density functional theory (DFT) as implemented in the Quantum-ESPRESSO package [20]. The electronic exchange-correlation potential was calculated within the generalized gradient approximation (GGA) in the scheme of Perdew-Burke-Ernzerhof (PBE) [21]. In all done total energy calculations, Vanderbilt-type ultra-soft pseudo-potential [22] was used to treat the potential seen by the valence electrons because of the nucleus and the frozen core electrons. The wave functions were expanded in a plane-wave basis set with a kinetic energy cut-off of 40 Ry. The electronic charge density was evaluated up to the kinetic energy cut-off of 400 Ry. Brillouin-zone integrations were performed using 10×10×10 *k*-points. Integration up to the Fermi surface was performed using the smearing technique [23] with smearing parameter $\sigma = 0.02$ Ry. Having obtained self-consistent solutions of Kohn-Sham equations, the lattice-dynamical properties were calculated within the framework of the self-consistent density functional perturbation theory (DFPT) [24,25]. Eight dynamical matrices were calculated on a 4×4×4 **q**-point mesh to obtain complete phonon dispersions and vibrational density of states. The dynamical matrices at arbitrary wave vectors were evaluated by means of a Fourier deconvolution on this mesh. Temperature dependence of the constant volume specific heat was calculated using the quasi-harmonic approximation (QHA) [26].

The elastic constants were obtained by calculating the total energy as a function of volume-conserving strains that break the cubic symmetry. Bulk modulus B, C_{44}, and shear modulus $C' = (C_{11}-C_{12})/2$ were calculated from hydrostatic pressure $e = (\delta, \delta, \delta, 0, 0, 0)$, tri-axial shear strain $e = (0, 0, 0, \delta, \delta, \delta)$ and volume-conserving orthorhombic strain $e = (\delta, \delta, (1+\delta)^{-2}\text{-}1, 0, 0, 0)$, respectively [27]. Hence, B was obtained from the following equation:

$$\frac{\Delta E}{V} = \frac{9}{2} B\delta^2 \tag{1}$$

Here V is the volume of unstrained lattice cell, and ΔE is the energy variation as a result of an applied strain with vector $e = (e_1, e_2, e_3, e_4, e_5, e_6)$. The shear modulus C' was obtained from the following expression:

$$\frac{\Delta E}{V} = 6C'\delta^2 + O\delta^3 \tag{2}$$

The above two expressions (1) and (2) yield $C_{11} = (3B + 4C')/3$, $C_{12} = (3B\text{-}2C')/3$. C_{44} was calculated from the following expression:

$$\frac{\Delta E}{V} = \frac{3}{4} C_{44}\delta^2 . \tag{3}$$

The details on the calculation of elastic constants have been described in our previous papers [28].

3. RESULTS AND DISCUSSION

3.1. Structural properties

The considered binary intermetallic Pd_3V and Pt_3V alloys were examined herein in the $L1_2$ phase. In the $L1_2$ phase, Pd_3V and Pt_3V are isostructural with Cu_3Au and crystallize in a cubic structure with the space group $Pm\bar{3}m$ (No 221 in the X-Ray Tables) as shown in Fig. 1. The crystalline structure of Pd_3V (Pt_3V) can be seen as four interpenetrating simple cubic sub-lattices, three occupied by Pd (Pt) atoms and one by V atoms. The atoms are positioned at the following Wyckoff positions: Pd(Pt): 3*c* (0, 1/2, 1/2) and V: 1*a* (0, 0, 0). As the first step, the equilibrium lattice constant was determined by minimizing the total energy with respect to different values of the lattice constant. Then, the total energy-volume data are fitted to the Murnaghan equation of state [29] to obtain the equilibrium lattice constant a_0, bulk modulus B_0 and first-order pressure derivative of the bulk modulus B'. The obtained values of a_0, B_0 and B' for the Pd_3V and Pt_3V compounds are tabulated in Table 1 along with the existing theoretical and experimental data for the sake of comparison. Our obtained values for both considered alloys are in good agreement with the available experimental measurements [16] and theoretical results [4,5,19]. The deviation of the herein calculated value of the lattice constant a_0 for Pt_3V from the existing measured one is about 1.7%, which illustrates the level of accuracy that can achieved in the modern DFT calculations. The discrepancy between our calculated bulk modulus value B for Pd_3V and the available measured one is about 4%. As can be seen, when going from Pd_3V to Pt_3V (i.e. when palladium (atomic radius R(Pd) = 1.79Å) is replaced by a larger platinum (atomic radius R(Pt) = 1.183Å), the lattice constant a_0 increase. It is worth to note here that the correlative relation between the unit cell volume V and the bulk modulus B (B~1/V) is absent here; Pt_3V has a large bulk modulus simultaneously with a large unit cell volume compared to Pd_3V.

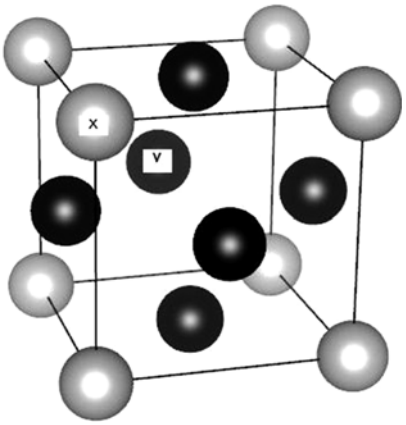

Fig. 1. Crystal structure of X_3V (X=Pd, Pt) alloys.

3.2. Elastic constants and related properties

The elastic properties of a cubic single-crystal are completely defined by three independents elastic constants, namely C_{11}, C_{12} and C_{44}. The C_{11} gives the resistance to the unidirectional compression (compression along the principal directions <100>), C_{44} presents the resistance to shear deformation across the (100) plane in the [110] direction, while C_{12} hasn't a simply physical meaning but its combination with C_{11} and C_{44} gives additional information about the elastic behaviour of materials. As an example, the tetragonal shear constant $C' = (C_{11} - C_{12})/2$ presents the resistance to shear deformation across the (110) plane along the $[1\bar{1}0]$ direction. The herein obtained values of C_{11}, C_{12}, C_{44} and C' for the considered materials are summarized in Table 1, along with available

Table 1. Calculated equilibrium lattice constant (a_0, in Å), total magnetic moment (M_{tot}, in μ_B), bulk modulus (B_0, in GPa), pressure derivative of the bulk modulus (B'), second order elastic constants (C_{ij}, in GPa) and tetragonal shear constant (C', in GPa) for the Pd_3V and Pt_3V alloys in the $L1_2$ structure

System	Ref.	a_0	M_{tot}	B_0	B'	C_{11}	C_{12}	C_{44}	C'
Pd_3V	This work[1]	3.908	1.35	186.72	4.85	263.58	148.28	107.02	57.65
	This work[2]			181.50		244.61	150.17	83.76	
	VASP [4]	3.889	-	-	-	265.287	156.456	88.383	72.76
	VASP [5]	3.902	-	-	-	-	-	-	-
	KKR [8]	-	1.29	-	-	-	-	-	-
	Exp. [11]	-	1.4	-	-	-	-	-	-
	Exp. [15]	-	-	-	-	271	-	68.5	-
	LSDF [19]	3.895	1.3	-	-	-	-	-	-
Pt_3V	This work[1]	3.936	1.29	239.02	5.17	345.15	185.96	135.97	79.60
	This work[2]			249.61		325.68	211.57	99.87	
	Exp. [16]	3.87	-	-	-	-	-	-	-
	LSDF [19]	3.88	1.3	-	-	-	-	-	-

[1]from energy-strain calculations
[2]from phonon calculations

experimental findings [15] and theoretical results [4] for the sake of comparison. Comparison of the elastic constants computed for Pd_3V and Pt_3V indicates that Pd_3V is less resistant to shear deformation and especially to compression since C_{11} and C_{44} are decreased at about 81.6 and 29.0 GPa, respectively. Our obtained values for the C_{11} and C_{12} for the Pd_3V compound are in reasonable agreement with the existing experimental [15] and theoretical [4] data. Our calculated value of C_{44} for the Pd_3V compound is relatively higher than the only measured one [15]. There are no available experimental or theoretical data for the elastic constants for the Pt_3V alloy in the $L1_2$ phase, so these predicted values are still waiting experimental confirmation. Our calculated values of the elastic constants for both herein considered materials satisfy the mechanical stability conditions for a cubic structure [30]:

$$C_{11}-C_{12}<0, C_{11}>0, C_{44}>0, C_{11}+2C_{12}>0 \quad (4)$$

The herein considered compounds are characterized by high values of C_{11} compared to C_{44}, C_{12} and C' (Table 1). The high values of C_{11} compared to the C_{44}, C_{12}, and C' ones is an indication of the more resistance to compression than to shear. By comparing between the values of C_{44} and those of C', one can deduce the lower resistance to shear across the (110) plane along the $[1\bar{1}0]$ direction than the resistance to shear across the (100) plane along the [010] direction in both studied compounds.

The Cauchy's pressure: $CP = (C_{12}-C_{44})$ [31] characterizes the predominant bonding type in crystals. A negative *CP* takes place for covalent materials with a strong directional character of bonds, whereas for metallic-like bonding the *CP* is positive. The *CP* of both herein studied materials is positive and this testify the metallicity of these two compounds in agreement with herein calculated band structure and that previously reported [4-6,8,19].

To further extends the elastic characteristics study of the Pd_3V and Pt_3V compounds, we have estimated the elastic wave velocities in the [100], [110] and [111] crystalline directions from the calculated single-elastic constants C_{ij}. Acoustic wave velocities in a material can be obtained from the Christoffel equation [32]. In a cubic structure, the sound wave velocities propagating in the [100], [010] and [111] directions are given by the following relations:

For [100] direction, the longitudinal and transverse wave velocities are defined as:

$$V_L^{100} = \sqrt{C_{11}/\rho} \quad (5)$$

$$V_L^{100} = \sqrt{C_{44}/\rho} \quad (6)$$

The elastic waves velocities, which propagate in the [110] direction are given as:

$$V_L^{110} = \sqrt{(C_{11}+C_{12}+2C_{44})/(2\rho)} \quad (7)$$

$$V_{T_1}^{110} = \sqrt{C_{44}/\rho} \quad (8)$$

$$V_{T_2}^{110} = \sqrt{(C_{11}-C_{12})/(2\rho)} \quad (9)$$

Finally, the elastic waves velocities along the [001] direction are written as:

$$V_L^{111} = \sqrt{(C_{11}+2C_{12}+4C_{44})/(3\rho)}$$

$$V_T^{111} = \sqrt{(C_{11}-C_{12}+C_{44})/(3\rho)} \quad (10)$$

Here ρ is the mass density, T and L stand for transverse and longitudinal polarization regardless the elastic wave propagation direction. The sound velocities deduced from the elastic constants C_{ij} are given in Table 2. From Table 2 data, it can be seen that the fastest and slowest longitudinal waves propagate along the [111] and [100] directions, respectively, whereas the fastest and slowest transverse waves propagate along the [100] and [110] directions, respectively.

Generally, large single-crystals are currently unavailable and consequently measurements of the individual elastic constants are impossible. The bulk modulus *B* and shear modulus *G* may be determined experimentally on the polycrystalline samples to characterize their mechanical properties. Theoretically, the calculated elastic constants of a single-crystal allows us to obtain its macroscopic mechanical properties of its bulk polycrystalline form, namely bulk modulus *B* and shear modulus *G* via the Voigt-Reuss-Hill approximations [33-35]. Here, Voigt and Reuss approximations represent extreme values, and Hill recommended that the arithmetic mean of these two limits is used as effective moduli in practice for polycrystalline samples. Their definitions for cubic systems can be found in Ref. 36, and their calculated values for the two studied materials

Table 2. Elastic waves velocities (in m/s) for different propagation directions for the Pd_3V and Pt_3V alloys in the $L1_2$ phase

System	V_L^{100}	V_T^{100}	V_L^{110}	V_{T1}^{110}	V_{T2}^{110}	V_L^{111}	V_T^{111}
Pd_3V[1]	5059	3224	5513	2801	2143	4925	2383
Pd_3V[2]	4872	2851	5223				
Pt_3V[1]	4463	2801	4814	2801	2143	4925	2383
Pt_3V[2]	4335	2400	4889				

[1]deduced from elastic constants calculations.
[2]deduced from phonon calculations.

Table 3. Calculated bulk modulus (B; in GPa), shear modulus (G; in GPa, the subscript R and V stand to Reuss and Voigt average), longitudinal, transverse and average sound velocity (V_l, V_t and V_m, respectively, in m/s), calculated from polycrystalline elastic moduli, and the Debye temperatures (T_D in K), calculated from the average sound velocity, for the Pd_3V and Pt_3V compounds

System	B	G_R	G_V	G	E	σ	V_l	V_t	V_m	T_D
Pd_3V	186.72	79.71	87.27	83.49	217.99	0.3054	5380	2847	3766	455
Pd_3V	239.02	105.95	113.42	109.69	285.41	0.3010	4716	2516	3328	399

are quoted in Table 3. Using the calculated values of the bulk and shear moduli we have evaluated the Young's modulus E and Poisson's coefficient σ using the known relations [36], and the obtained results are summarized in Table 3.

Pugh's B/G ratio empirical criterion [37] is one of the widely used to provide information about brittle (ductile) nature of materials. If $B/G > 1.75$, ductile behavior is predicted; otherwise, the material behaves in a brittle manner. According to the values of B and G shown in Tables 1 and 3, the B/G ratio is equal to 2.34 and 2.18 for Pd_3V and Pt_3V, respectively, indicating a ductile nature of both considered materials and thus they will be resistant to thermal shocks; their mechanic properties decrease slowly with increasing temperature.

The obtained values for the Poisson's ratio σ, 0.3054 for Pd_3V and 0.3010 for Pt_3V, confirm that both herein studied materials belong to metallic-like systems since for ductile metallic materials σ is typically 0.33 [38].

Since strong correlation between bulk modulus and hardness of materials has been confirmed in several papers [39], we expect from our obtained results that Pt_3V should exhibit higher hardness than Pd_3V. The Young's modulus E measures the response to an uniaxial stress averaged over all directions and is used often to denote a measure of stiffness, i.e. the larger is the value of E, the stiffer is the material. According to this Pt_3V is stiffer than Pd_3V. The investigation of the stiffness can be completed by providing the microhardness parameter (H), given by the following relation [40]:

$$H = \frac{(1-2\sigma)E}{6(1+\sigma)} \tag{11}$$

The calculated H values are 10.83 and 14.55 GPa for Pd_3V and Pt_3V, respectively. These estimated values reveal that $H(Pt_3V) > H(Pd_3V)$, but both compounds exhibit rather small hardness (≈10-14 GPa).

Practically, all known crystals are elastically anisotropic, and a proper description of such anisotropic behavior has an important implication in engineering science as well as in crystal physics since the elastic anisotropy could introduce microcracks in materials [41,42]. Moreover, recent research demonstrates that the elastic anisotropy of crystals has a significant influence on the nanoscale precursor textures in alloys [43,44]. Therefore, several criteria have been developed to investigate the elastic anisotropy.

Although the herein considered compounds are cubic, they possess anisotropic elastic properties, which can be analyzed in three ways. First, the degree of anisotropy can be evaluated from the values of the upper (Voigt, G_V) and lower (Reuss, G_R) shear moduli by introducing the so-called anisotropy factor A_G [45]: $A_G = (G_V - G_R)/(G_V + G_R)$. A value of zero represents elastic isotropy and a value of 1 (100%) is the largest possible anisotropy. Numerical calculation with the given values of G_V and G_R in Table 3 yields $A_G^{Pd_3V} = 0.045$ (4.5%) and $A_G^{Pd_3V} = 0.034$ (3.4%). These values indicate that these compounds are characterized by weak shear anisotropy.

The above elastic anisotropy criteria quantify the anisotropy degree from shear contribution. In order to quantify the extent of the anisotropy accurately, a new and more universal index A^U has been proposed by Ranganathan and Ostoja-Starzewski [46] to measure the single-crystal anisotropy accounting for both bulk and shear contributions, where the A^U is defined as follows: $A^U = 5G_V/G_R + B_V / B_R - 6$. For isotropic crystals, the universal index is equal to zero ($A^U = 0$); the deviations of A^U from zero definite the extent of crystal anisotropy. The listed values in Table 3 reveal that A^U (Pd_3V) = 0.47 and A^U (Pd_3V) = 0.35. So, the studied materials are characterized by a noticeable anisotropy.

The third way of treating elastic anisotropy is to plot a three-dimensional dependence of the Young's modulus E on given direction in a crystal. Three-dimensional (3D) surface representation of the elastic moduli is an effective method to visualize the elastic anisotropy of a material along its crystallographic directions. In 3D representation, an isotropic system would exhibit a spherical shape, and a deviation from spherical shape indicates the degree of anisotropy. So, for a deep look into the peculiar features of the elastic anisotropy of our herein studied materials we have plotted in Fig. 2 their direction-dependent Young's modulus surface using the following relation [47]:

$$E = \frac{1}{\{S_{11} + 2[S_{11} - S_{12} - 1/(2S_{44})](n_1^2 n_2^2 + n_2^2 n_3^2 + n_3^2 n_1^2)\}} \tag{12}$$

where the S_{ij} are the elastic compliance constant that can be obtained through an inversion of the elastic constant matrix, and n_1, n_2 and n_3 are the directional cosines with respect to the x-, y- and z-axes, respectively. The shape of the surfaces plotted in Fig. 2 is far from spherical and exhibits a noticeable anisotropy. We have plotted also in Fig. 2 the cross-section of these surfaces in the (001), (010) and (110) coordinate planes. In both considered compounds the highest value of the Young's modulus E_{max} is realized for the external stress

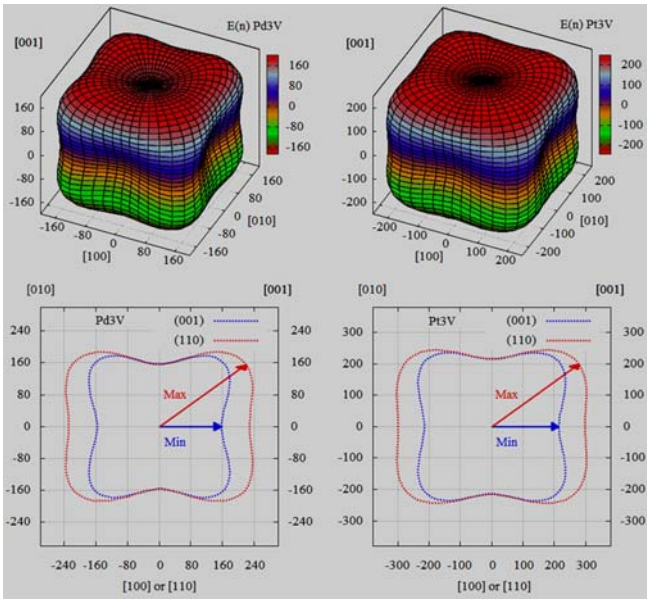

Fig. 2. Visualizations of the Young's moduli surfaces (left panels) and their cross-sections in the (100), (010) and (001) planes (right panels) for the Pd_3V and Pt_3V alloys in the $L1_2$ phase. The axes units are in GPa.

applied along the crystallographic axes *a*, *b* and *c* ([100], [010] and [001] directions), and the lowest value E_{min} is for the stress along the [111] direction. The lowest value, E_{min}, is about 58% of the highest value of the Young's modulus, E_{max}, in Pd_3V and it is 63% in Pt_3V, indicating noticeable anisotropic elastic behavior in these two materials.

Debye temperature, which determines the thermal characteristics of a material, can be estimated from the average sound velocity in an isotropic material [48]. The obtained values of the longitudinal, transverse and average sound velocities (V_l, V_t and V_m, respectively), and the Debye temperature θ_D for polycrystalline Pd_3V and Pt_3V are gathered in Table 3.

3.3. Electronic properties

Spin-polarized band structures of the Pd_3V and Pt_3V alloys for spin-up (majority-spin) and spin-down (minority-spin) alignments are shown in Fig. 3 along the high symmetry directions in the first Brillouin zone together with their total densities of states. Both spin-up and spin-down band structures show that no energy band gap in these materials indicating their metallic character. Total and atomic-resolved *l*-projected densities of states (DOSs) for both herein considered alloys as calculated for equilibrium geometries are presented in Fig. 4. DOSs diagrams show no energy gap at the Fermi level for both considered alloys. This confirms that the majority-spin (up) and minority-spin (down) exhibit metallic behavior. Total

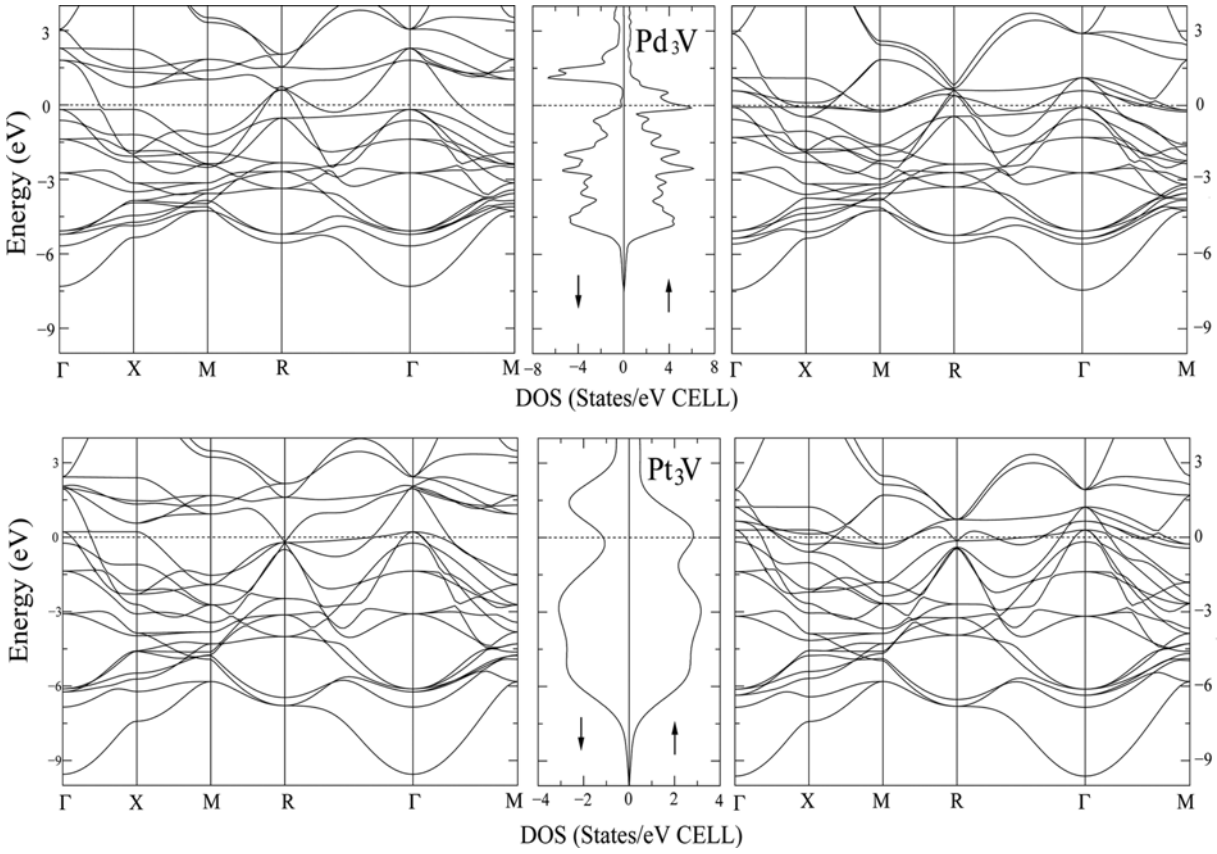

Fig. 3. Calculated band structure along several selected high-symmetry directions in the Brillouin zone for the Pd_3V and Pt_3V alloys in the $L1_2$ phase. The left panels are majority-spin (up) bands and the right panels the minority-spin (down). The Fermi level is set at zero energy.

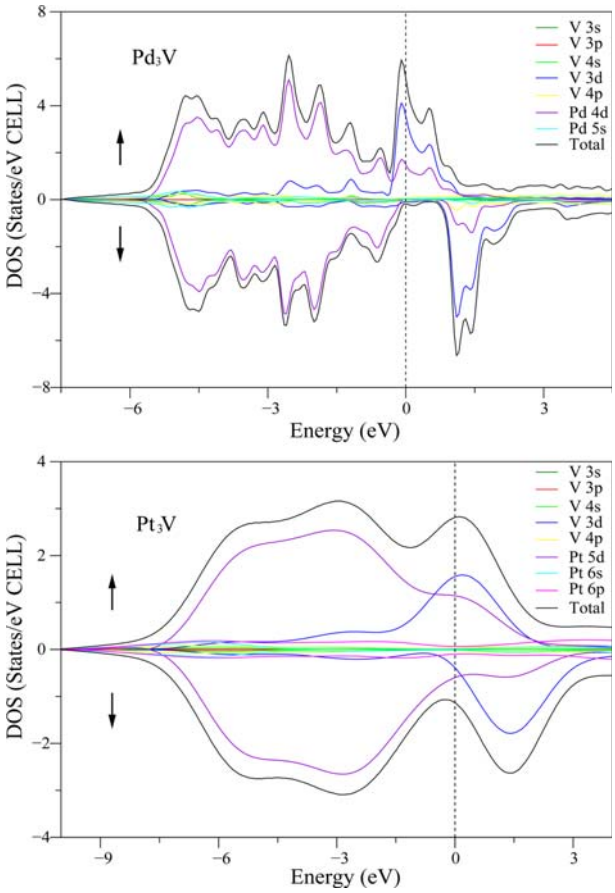

Fig. 4. Spin-dependent total and partial densities of states of the Pd_3V and Pt_3V ferromagnetic alloys. The Fermi level is set at zero energy.

density of states at the Fermi level $N^{total}(E_F)$ for Pd_3V and Pt_3V in $L1_2$ phase are found to be 5.179 and 2.814 states/eV/unit-cell, respectively, for spin-up and 0.176 and 1.133 states/eV/unit-cell, respectively, for spin-down. These results are in good agreement with the reported results by Tobola *et al*. [8] for Pd_3V; they found $N^{total}(E_F) = 5.331$ states/eV/unit-cell for spin-up, and 0.279 states/eV/unit-cell for spin-down. Our results are also in good accordance with those reported by Kübler [19]; they obtained $N^{total}(E_F) = 4.700$ (3.900) states/eV/unit-cell for spin-up and 0.200 (0.600) states/eV/unit-cell for spin-down for Pd_3V (Pt_3V). The predominant contributions to the density of states at the Fermi level comes from the V-3*d* and Pd- 4*d* (Pt-5*d*) states for Pd_3V (Pt_3V). The electronic states above Fermi level are mainly dominated by the Pd-4*d* states for Pd_3V and the Pt-5*d* states for Pt_3V (see Fig. 4). The structures situated below Fermi level for Pd_3V (Pt_3V) arise essentially from the V-3*d* and Pd-4*d* (Pt-5*d*) states.

The calculated values of the total magnetic moments (M_{tot}) for the Pd_3V and Pt_3V alloys are given in Table 1 along with the existing experimental measurements [11] and theoretical results [8,19] for comparison. Our calculated magnetic moments are in good agreement with these available experimental and theoretical findings.

3.4. Vibrational properties

Lattice-dynamical properties of the Pd_3V and Pt_3V alloys were herein studied using the linear-response approach as implemented in the Quantum-ESPRESSO package [20]. Figure 5 shows the calculated phonon dispersion curves along several symmetry lines in the first Brillouin zone together with their corresponding total and projected phonon densities of states (DOS) for Pd_3V and Pt_3V in the $L1_2$ phase. As the unit cell of the $L1_2$ structure contains four atoms, so there are 12 phonon branches, three acoustical and nine optical. In our previous paper, we have reported that the phonon branches reduce some symmetry directions [49]. Because of the symmetry, the distinct number of phonon branches is reduced along the principal symmetry directions Γ-X and M-R-Γ. As can be seen from Fig. 5, all phonon modes have positive frequencies indicating the dynamical stability of these compounds in the $L1_2$ structure. For both studied materials, the separation between the acoustical and optical branches is not sufficient to create a gap. The low-frequency part of the phonon DOS in the $L1_2$ phase consists mostly of the contribution of the heavier Pd atoms for Pd_3V and Pt atoms for Pt_3V, while the contribution of lighter V atoms appears only at the uppermost frequency range about 4 THz for both alloys. Some numerical values at high symmetry point Γ, *X*, *M* and *R* are reported in Table 4. There are no available theoretical or experimental data for the phonon frequencies for the herein considered materials to be compared

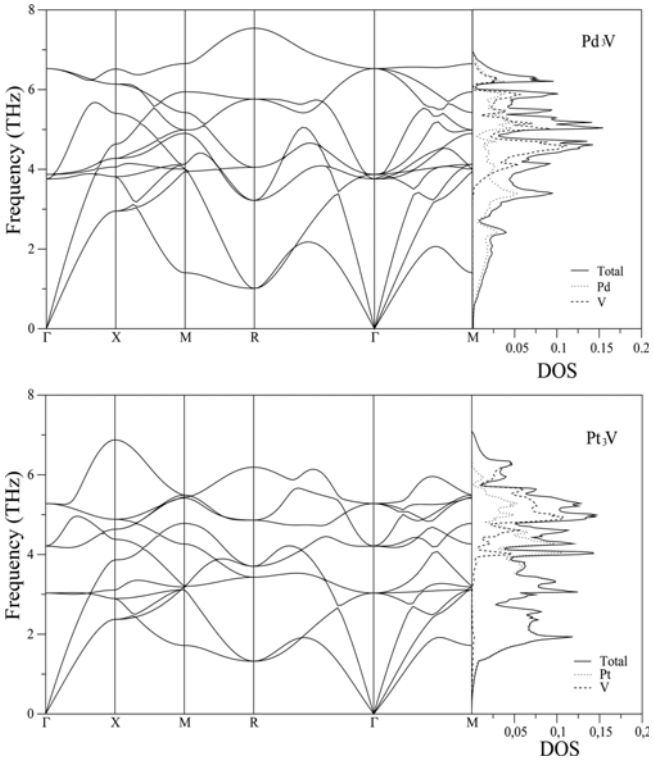

Fig. 5. Calculated phonon dispersion curves and density of states (DOS) for the Pd_3V and Pt_3V alloys in the $L1_2$ phase.

Table 4. Phonon frequencies (in THz) obtained at high symmetry points for the Pd_3V and Pt_3V alloys in the $L1_2$ structure

High symmetry point	Pd_3V	Pt_3V
Γ	3.758, 3.873, 6.528	3.032, 4.211, 5.279
X	2.953, 3.815, 4.057, 4.275, 4.635, 5.402, 6.137, 6.515	2.372, 2.893, 3.110, 3.865, 4.380, 4.634, 4.883, 6.876
M	1.403, 3.949, 4.005, 4.129, 4.903, 4.987, 5.426 5.944, 6.650	1.720, 3.117, 3.185, 3.204, 4.263, 4.780, 5.418, 5.443, 5.490
R	1.010, 3.218, 4.049, 5.763, 7.540	1.323, 3.430, 3.705, 4.863, 6.191

with our present results. Our phonon calculations are in good agreement with our earlier work [50] which belong to the same space group and structure.

Elastic wave velocities for the $L1_2$ Pd_3V and Pt_3V alloys can be deduced from the slope of the acoustic phonon branches for small wave vectors near the Γ point [51]. The deduced sound velocity values of the LA and TA phonon branches along the [001] direction ($V_L^{[001]}$, $V_T^{[001]}$) and of the LA phonon branch along the [110] direction ($V_L^{[110]}$) for the Pd_3V and Pt_3V materials are listed in Table 2. These findings are in good agreement with the ones deduced from the elastic constants (see Table 2). Using eqs. (5), (6) and (7) we deduced the values of the elastic constants C_{11}, C_{44} and C_{12} from these calculated elastic wave velocities. The deduced values for the elastic constants from the acoustic phonon branches are given in Table 1. The elastic constants values deduced from the acoustic phonon branches are in reasonable agreement with those calculated from total energy-strain variations. On other side, one can see that the bulk modulus values evaluated from the single-crystal elastic constants calculated by two different approaches: total energy-stain and acoustic phonon branches are in good agreement with its value derived from the Murnaghan equation of state. This might be an estimate of the reliability and accuracy of our calculated elastic constants for the Pd_3V and Pt_3V alloys.

The knowledge of the entire phonon spectrum granted by DFPT makes possible the calculation of several important thermo-dynamical properties as function of temperature T. Temperature dependence of the constant-volume specific heat C_V for the Pd_3V and Pt_3V alloys in the $L1_2$ structure are determined within the quasi-harmonic approximation based on the calculated phonon dispersion relations and depicted in Fig. 6. It is found that at low temperature C_V increases rapidly with increasing temperature, while at high temperature, for both alloys, it approaches the classical asymptotic Dulong-Petit limit [52] value of 12R, where R is the perfect gas constant (R = 8.3145 $Jmol^{-1}$). The calculated value of C_V at T = 300 K is 95.94231 and 96.24614 $Jmol^{-1}K^{-1}$ for Pd_3V and Pt_3V, respectively. Unfortunately, there are no available data in the literature in order to testify our results for C_V of the herein studied materials.

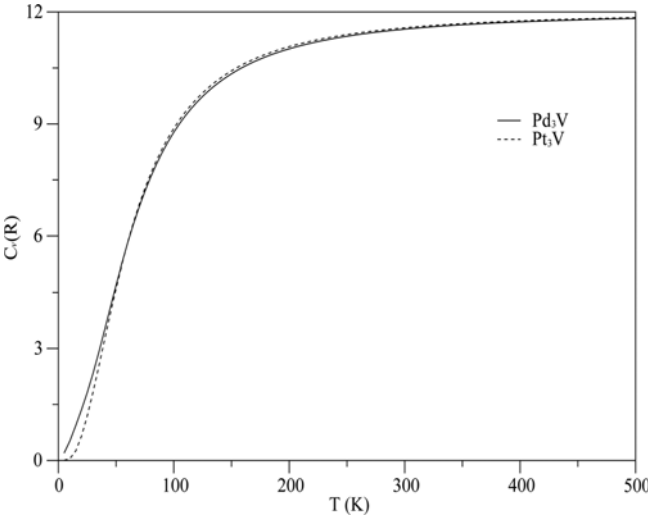

Fig. 6. Calculated specific heat capacity at constant volume versus temperature for the Pd_3V and Pt_3V alloys in the $L1_2$ phase.

4. CONCLUSIONS

In summary, we have performed PP-PW calculations to study the structural, elastic, electronic and lattice-dynamical properties of the binary intermetallic Pd_3V and Pt_3V in the $L1_2$ phase. Form the present study of the Pd_3V and Pt_3V we may draw the following main conclusions:

(1) The obtained values for the equilibrium lattice parameters are in good agreement with the existing experimental data which testify the accuracy and viability of the herein chosen calculation method.

(2) Analysis of the computed single-crystal elastic constants show that the considered materials are mechanically stable.

(3) Calculated bulk modulus, Young's modulus and microhardness parameter show that Pt_3V will be stiffer than Pd_3V.

(4) According to Pugh's indicator of brittle/ductile, both herein studied materials should behave as ductile materials.

(5) According to Poisson's ratio and Cauchy's pressure values, we can assume the metallic-like bonding in these two compounds.

(6) Analysis of three different indexes of elastic anisotropy reveals that these materials have a noticeable elastic anisotropy.

(7) Calculated electronic band structure and their corresponding total and atomic-resolved densities of states, and total magnetic moment are in good agreement with the existing data. Band structure and density of states diagrams confirm the metallicity of the Pd_3V and Pt_3V alloys in the $L1_2$ phase.

(8) Phonon dispersion curves and their corresponding total and projected densities of states for the Pd_3V and Pt_3V alloys in the $L1_2$ phase were calculated for the first time in the framework of the density-functional perturbation theory. Elastic constants values deduced from the acoustic phonon spectra are in reasonable agreement with those calculated using total energy-strain variations. Temperature dependence of the constant-volume

specific heat is determined from the obtained phonon spectra using the quasi-harmonic approach.

ACKNOWLEDGMENT

This work was supported by the Ahi Evran University Research Project Unit under Project No FBE-11-29 and the Gazi University Research Project Unit under Project No 05/2012-62, 05/2012-63, 05/2012-07, 05/2012-08.

REFERENCES

1. T. Tian, X. F. Wang, and W. Li, *Solid State Commun.* **156**, 69 (2013).
2. C. Colinet and A. Pasturel, *Calphad* **26**, 563 (2002).
3. O. Lebacq, A. Pasturel, D.N. Manh, A. Finel, and R. Caudron, *J. Alloy. Compd.* **264**, 31 (1998).
4. T. Wang, P. Chen, Y. Deng, and B. Tang, *Trans. Nonferr. Met. Soc. China* **21**, 388 (2011).
5. R. Hirschl, J. Hafner, and Y. Jeanvoine, *J. Phys.: Condens. Matter* **13**, 3545 (2001).
6. Z. W. Lu, B. M. Klein, and A. Zunger, *Phys. Rev. Lett*. **75**, 1320 (1995).
7. C. Wolverton and A. Zunger, *Phys. Rev. B* **52**, 8813 (1995).
8. J. Tobola and P. Pécheur, *J. Alloy. Compd.* **317-318**, 428 (2001).
9. D. Brown, M. D. Crapper, K. H. Bedwell, M. T. Butterfield, S. J. Guilfoyle, A. E. R. Malins, and M. Petty, *J. Phys.: Condens. Matter* **9**, 9435 (1997).
10. B. S. Mun, M. Watanabe, M. Rossi, S. Stamenkovic, N. M. Markovic, and P. N. Ross, *J. Chem. Phys.* **123**, 204717 (2005).
11. A. W. Sheikh and G. Williams, *Phys. Rev. B* **28**, 5307 (1983).
12. E. Cabet, A. Pasturel, F. Ducastelle, and A. Loiseau, *Phys. Rev. Lett.* **76**, 3140 (1996).
13. A. Loiseau and E. Cabet, *Journal de Physique IV* **3**, 5021 (1993).
14. D. Morgan. A. van de Walle, G. Ceder, J.D. Althoff, and D. de Fontaine, *Modelling Simul. Mater. Sci. Eng.* **8**, 259 (2000).
15. M. E. Manley, B. Fultz, and L. J. Nagel, *Philos. Mag. B* **80**, 1167 (2000).
16. R. Jesser, A. Bieber, and R. Kuentzler, *J. Phys-Paris* **42**, 1157 (1981).
17. F. Solal, R. Caudron, F. Ducastelle, A. Finel, and A. Loiseau, *Phys. Rev. Lett.* **58**, 2245 (1987).
18. A. van de Walle and G. Ceder, *Phys. Rev. B* **61**, 5972 (2000).
19. J. Kübler, *J. Magn. Magn. Mater.* **45**, 415 (1984).
20. P. Giannozzi, S. Baroni, N. Bonini, M. Calandra, R. Car, C. Cavazzoni, D. Ceresoli, G.L. Chiarotti, M. Cococcioni, I. Dabo, A. Dal Corso, S. Fabris, G. Fratesi, S. de Gironcoli, R. Gebauer, U. Gerstmann, C. Gougoussis, A. Kokalj, M. Lazzeri, L. Martin-Samos, N. Marzari, F. Mauri, R. Mazzarello, S. Paolini, A. Pasquarello, L. Paulatto, C. Sbraccia, S. Scandolo, G. Sclauzero, A.P. Seitsonen, A. Smogunov, P. Umari, and R. M. Wentzcovitch, *J. Phys.: Condens. Matter* **21**, 395502 (2009).
21. P. Perdew, K. Burke, and M. Ernzerhof, *Phys. Rev. Lett.* **77**, 3865 (1996).
22. D. Vanderbilt, *Phys. Rev. B* **41**, 7892 (1990).
23. M. Methfessel and A.T. Paxton, *Phys. Rev. B* **40**, 3616 (1989).
24. S. Baroni, P. Giannozzi, and A. Testa, *Phys. Rev. Lett.* **58**, 1861 (1987).
25. S. Baroni, S. de Gironcoli, A. Dal Corso, and P. Giannozzi, *Rev. Mod. Phys.* **73**, 515 (2000).
26. E. I. Isaev, *QHA Project*, http://qe-forge.org/qha (accessed May 25, 2013).
27. S. Q. Wang and H. Q. Ye, *Phys. Stat. Sol. (b)* **240**, 45 (2003).
28. Ş. Uğur, G. Uğur, F. Soyalp and R. Ellialtıoğlu, *J. Rare Earth* **27**, 664 (2009).
29. F. D. Murnaghan, *Proc. Natl. Acad. Sci. USA* **50**, 697 (1944).
30. J. Wang, S. Yip, S. R. Phillpot, and D. Wolph, *Phys. Rev. Lett.* **7**, 4182 (1993).
31. R. A. Johnson, *Phys. Rev. B* **37**, 3924 (1988).
32. L. D. Landau, E. M. Lifschitz, *Theory of Elasticity, Course of Theoretical Physics,* Pergamon Press, New York (1980).
33. W. Voigt, *Lehrbuch der Kristallphysik*, Taubner, Leipzig (1928).
34. A. Reuss and Z. Angew, *Math. Mech*. **9**, 55 (1929).
35. R. Hill, *Proc. Phys. Soc. London, Sect. A* **65**, 349 (1952).
36. M. J. Mehl, B. M. Klein, D. A. Dimitri, and A. Papaconstantopoulos, *Intermetallic Compounds: Principles and Practice*, *Volume I: Principles, J. H. Westbrook and R. L. Fleischer*, (eds. J. Wiley and Sons), London (1995).
37. S. F. Pugh, *Phil. Mag*. **45**, 823 (1954).
38. J. Haines, J. Leger, and G. Bocquillon, *Ann. Rev. Mater. Res*. **31**, 1 (2001).
39. I. R. Shein, K. I. Shein, and A. L. Ivanovskii, *J. Nucl. Mater.* **361**, 69 (2007).
40. Y. El Sayed, A. El-Adawy, and N. El-Kheshkhany, *Solid State Commun.* **139**, 108 (2006).
41. R. Ravindran, L. Fast, P. A. Korzhavyi, B. Johansson, J. Wills, and O. Eriksson, J. *App. Phys.* **84**, 4891 (1998).
42. D. H. Chung and W. R. Buessem, *Anisotropy in Single Crystal Refractory Compound,* (eds. F.W. Vahldiek and A. Mersol), Plenum, New York (1968).
43. P. Llioveras, T. Castán, M. Porta, A. Planes, and A. Sexena, *Phys. Rev. Lett*. **100**, 165707 (2008).
44. P. Rong-Kai, M. Li, B. Nan, W. Ming-Hui, L. Peng-Bo, T. Bi-Yu, P. Li-Ming, and D. Wen-Jiang, *Phys. Scr.* **87**, 015601 (2013).
45. M. G. Brik and A. M. Srivastava, *Mater. Chem. Phys.* **132**, 6 (2012).
46. S. I. Ranganathan and M. Ostoja-Starzewski, *Phys. Rev. Lett*. **101**, 55504 (2008).
47. A. Cazzani and M. Rovati, *Int. J. Solids Struct*. **40**, 1713 (2003).
48. A. Bouhemadou, *Physica B* **403**, 2707 (2008).
49. Ş. Uğur, *Mater. Sci. Eng. B*, **162**, 116 (2009).
50. N. Arıkan, *J. Phys. Chem. Sol*. **74**, 794 (2013).
51. G. P. Srivastava, *The Physics of Phonons,* Bristol: Adam Hilger (1990).
52. A. T. Petit and P. L. Dulong. *Ann. Chim. Phys.* **10**, 395 (1819).